Lack of acrosome formation in mice lacking a Golgi protein, GOPC

Ryoji Yao*, Chizuru Ito†, Yasuko Natsume*, Yoshinobu Sugitani*, Hitomi Yamanaka*, Shoji Kuretake‡, Kaoru Yanagida‡, Akira Sato‡, Kiyotaka Toshimori†, and Tetsuo Noda*§¶‖**

*Department of Cell Biology, Japanese Foundation for Cancer Research (JFCR) Cancer Institute, 1-37-1 Kami-Ikebukuro, Toshima-Ku, Tokyo 170-8455, Japan; †Department of Anatomy and Reproductive Cell Biology, Miyazaki Medical Collage, Kiyotake, Miyazaki 889-1692, Japan; ‡Department of Obstetrics and Gynecology, Fukushima Medical Collage, 1 Hikarigaoka, Fukushima 960-1295, Japan; §Department of Molecular Genetics, Tohoku University School of Medicine, 2-1 Seiryo-cho, Aoba-Ku, Sendai 980-8575, Japan; ¶Core Research for Evolutional Science and Technology (CREST), Japan Science and Technology Corporation, 4-1-8 Motomachi, Kawaguchi 332-0012, Japan; and ‖Mouse Functional Genomics Research Group, Institute of Physical and Chemical Research (Japan) (RIKEN) Genomic Sciences Center, 214 Maeda-cho, Totsuka-ku, Yokohama, Kanagawa 244-0804, Japan

Edited by Kai Simons, Max Planck Institute of Molecular Cell Biology and Genetics, Dresden, Germany, and approved June 19, 2002 (received for review January 31, 2002)

The acrosome is a unique organelle that plays an important role at the site of sperm–zona pellucida binding during the fertilization process, and is lost in globozoospermia, an inherited infertility syndrome in humans. Although the acrosome is known to be derived from the Golgi apparatus, molecular mechanisms underlying acrosome formation are largely unknown. Here we show that Golgi-associated PDZ- and coiled-coil motif-containing protein (GOPC), a recently identified Golgi-associated protein, is predominantly localized at the trans-Golgi region in round spermatids, and male mice in which *GOPC* has been disrupted are infertile with globozoospermia. The primary defect was the fragmentation of acrosomes in early round spermatids, and abnormal vesicles that failed to fuse to developing acrosomes were apparent. In later stages, nuclear malformation and an abnormal arrangement of mitochondria, which are also characteristic features of human globozoospermia, were observed. Interestingly, intracytoplasmic sperm injection (ICSI) of such malformed sperm into oocytes resulted in cleavage into blastocysts only when injected oocytes were activated. Thus, GOPC provides important clues to understanding the mechanisms underlying spermatogenesis, and the GOPC-deficient mouse may be a unique and valuable model for human globozoospermia.

The acrosome is a unique structure of the mature spermatozoon, which plays an important role at the site of sperm–zona pellucida binding during the fertilization process. The biogenesis of the acrosome takes place during the initial phase of spermatid development, when numerous proacrosomic granules are formed from trans-Golgi stacks and accumulate in the concave region near the trans-Golgi stacks—i.e., medulla. The small granules fuse with each other to form a single large acrosomic granule that associates with the nuclear envelope (1). During the subsequent cap phase, the acrosome increases its size and begins to spread over the anterior nuclear pole. The nucleus changes its shape during the subsequent acrosomic phase, which is followed by caudal migration of mitochondria during the maturation phase. Although the morphogenic change of the acrosome in spermatogenesis has been well documented, its molecular basis is still largely unknown.

Globozoospermia (also called round-headed spermatozoa) is a human infertility syndrome caused by spermatogenesis defects (2–4). The most prominent feature of globozoospermia is the malformation of the acrosome, and, in the most severe cases, the acrosome is totally absent. Globozoospermia is also characterized by abnormal nuclear shape as well as abnormal arrangement of the mitochondria of the spermatozoon (5). Although globozoospermia is thought to be an inherited disorder (2), the etiology of globozoospermia is not known.

We have identified mouse Golgi-associated PDZ- and coiled-coil motif-containing protein (GOPC) as a Frizzled-interacting protein, and propose that GOPC may have a role in vesicle transport from the Golgi apparatus (6). GOPC contains one PDZ domain, two coiled-coil motifs, and two evolutionarily conserved domains. The PDZ domain of GOPC is required for its Frizzled binding, whereas coiled-coil motifs and conserved domains are required for its Golgi localization. Charest *et al.* (7) reported that FIG (fused in glioblastoma), a possible human homologue of GOPC with 92.3% identity, interacted with syntaxin-6, supporting the idea that GOPC may play a role in vesicle transport from the Golgi apparatus. In the present study, we have investigated the biological role of GOPC by gene targeting to generate mice bearing a null allele of *GOPC*, and found that GOPC-deficient male mice were infertile with globozoospermia. The spermatozoa from GOPC-deficient mice showed complete lack of acrosomes, which is because of the failure of vesicle transport from the Golgi apparatus.

CELL BIOLOGY

Materials and Methods

Reverse Transcription (RT)-PCR and Northern Blot Analysis. RNA from various mouse tissues was isolated by using a FastTrack kit (Invitrogen) and cDNA synthesis and PCR were performed by using a cDNA cycle kit (Invitrogen). The primers were synthesized based on the sequences of exons 2 and 3. The sequences of primers were as follows: exon 2 primer, 5′-CCACTCAGCTTCAGCTTCATGCC-3′; exon 3 primer, 5′-AGCCTGGAGAACAGCTATGTGCC-3′.

For Northern blot analysis, 4 μg of poly(A)$^+$ RNA was separated in a 1% formaldehyde/agarose gel and transferred to Duralon-UV nylon membrane (Stratagene) according to the manufacturer's instructions. The filter was hybridized with the 0.9-kb [α-^{32}P]dCTP-labeled GOPC cDNA encompassing the PDZ domain.

Immunoblot Analysis. Tissue extracts were prepared by homogenization in Nonidet P-40 buffer (20 mM Tris·HCl, pH 8.0/137 mM NaCl/1% Nonidet P-40/10% glycerol) supplemented with 1 mM phenylmethylsulfonyl fluoride, 1 μg/ml leupeptin, 1 μg/ml aprotinin, and 0.5 mM DTT in a Dounce homogenizer. The homogenates were centrifuged at 13,000 rpm for 15 min and protein concentrations were determined by the Bio-Rad protein assay. Twenty-five micrograms of protein lysates was separated in SDS/PAGE and electrotransferred to nitrocellulose. Antiserum against GOPC has been described (6). The bound antibody was detected by ECL Western blotting detection reagents (Amersham Pharmacia Biotech).

This paper was submitted directly (Track II) to the PNAS office.

Abbreviations: GOPC, Golgi-associated PDZ- and coiled-coil motif-containing protein; RT-PCR, reverse transcription–PCR; ICSI, intracytoplasmic sperm injection.

**To whom reprint requests should be addressed. E-mail: tnoda@ims.u-tokyo.ac.jp.

Gene Targeting. A genomic clone encompassing exons 2, 2b, 3, and 4 of *GOPC* was isolated from the 129 genomic library and a targeting vector in which nLacZ and floxed pMC1neo poly(A) replaced exons 2, 2b, and 3 was constructed. A nLacZ fragment was inserted in frame in the *Pvu*I site of exon 2, and the DT-A fragment was ligated at the 3′ end of the targeting vector for negative selection. The targeting vector was linearized by *Not*I digestion before electroporation into J1 ES cells. Of 274 G418-resistant clones, 5 clones had undergone homologous recombination as determined by Southern blot analysis. Two clones were injected into C57BL/6 blastocysts, resulting in the birth of male chimeric mice. Germ-line transmission of the disrupted *GOPC* allele was achieved by mating with C57BL/6 females.

Immunohistochemistry. Adult testes from wild-type and *GOPC*$^{-/-}$ mice were fixed with 4% paraformaldehyde (PFA) by perfusion and immersed for 20 hr at 4°C. The testes were rinsed in phosphate buffer (PB), washed through a sucrose gradient (10-, 20-, and 30% in PB), and embedded in OCT compound (Miles, Elkhart, IN). Frozen sections were immunostained with anti-GOPC serum, followed by Cy3-conjugated anti-rabbit IgG (Cappel). Nuclei were stained with 4′,6-diamidino-2-phenylindole. To isolate spermatogenic cells, testes were removed, dissected with scissors, and digested with collagenase followed by trypsin (8). Cells were washed several times, plated onto poly-L-lysine coated coverslips, fixed, and stained as detailed above.

Conventional Transmission Electron Microscopy. Adult testes were fixed with 2% glutaraldehyde in 0.2 M cacodylate buffer. After washing in the same buffer, the tissues were cut into small pieces, immersed in the same fixative for 2 hr at 4°C, rinsed, and then fixed with OsO_4. Thereafter, the samples were dehydrated through a graded ethanol series, and then embedded in Epon 812. Ultrathin sections were cut on an ultramicrotome (model 2088, LKB-Produkter, Bomma, Sweden), and stained with uranyl acetate and lead citrate in a LKB 2168 ultrostainer. Observation was performed with a Hitachi H-7100 transmission electron microscope (TEM).

Immunoelectron Microscopy. Adult testes were fixed with periodate/lysine/2% paraformaldehyde (PLP) fixative by perfusion through the left ventricle, and then immersed in the same fixative for 20 hr at 4°C. The testes were rinsed in PB, washed through a sucrose gradient (10-, 15-, and 20% in PB), and then incubated in 20% sucrose:OCT compound (1:1) overnight at 4°C. The testes were then embedded in the 1:1 mixture of 40% sucrose/OCT compound, quickly frozen in liquid nitrogen, and sectioned at 6-μm thickness on a Leitz cryostat (model 1720, Wetzlar, Germany). Slides were dried, treated with 0.3% H_2O_2 in methanol for 30 min, and blocked with 10% goat serum in PBS for 30 min. After blocking, sections were incubated with the anti-GOPC serum (1/25) at 4°C overnight and washed in PBS. The sections were then incubated with the horseradish peroxidase-conjugated Fab′ fragment of goat anti-rabbit IgG (Protos Immunoresearch, San Francisco), fixed with 0.5% glutaraldehyde, reacted with 0.05% diaminobenzidine/H_2O_2, and postfixed with 1% OsO_4. They were dehydrated, embedded, and cut as described above. Ultrathin sections were examined without counterstaining with a Hitachi H-7100 TEM. Control experiments were done with normal rabbit serum instead of the GOPC antibody. Nonspecific staining was also checked by omitting the incubation step with the first antibody.

Intracytoplasmic Sperm Injection (ICSI). ICSI and oocyte stimulation were performed essentially as described (9). Briefly, spermatozoa were prepared from caudae epididymides of F_2 *GOPC* mice, suspended in human tubal fluid (HTF) medium (Irvine Scientific), and then transferred to HTF medium containing 8% polyvinylpyrrolidone (Sigma). A spermatozoon was drawn, tail first, into the pipette and injected. Where indicated, oocytes were stimulated electrically 30 min after ICSI by a single, square dc pulse (1.5 kV/cm, 100 μs). Sperm-injected oocytes were incubated in HTF medium for 6 h and then cultured in KSOM (K simplex optimized median) until injected oocytes were developed to the blastocyst stage. Developed oocytes were fixed, stained, and examined cytologically by phase-contrast microscopy.

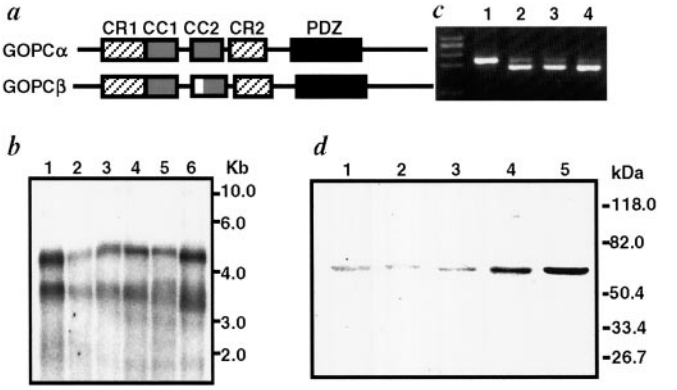

Fig. 1. Structure and expression of GOPC. (*a*) Structures of GOPCα and GOPCβ. The white box indicates the position at which the 8-aa insertion is found in GOPCβ. CR, conserved region; CC, coiled-coil motif; PDZ, PDZ domain. (*b*) Northern blot analysis of GOPC. Aliquots (4 μg) of poly(A) were probed with GOPC cDNA. Lanes: 1, brain; 2, lung; 3, heart; 4, liver; 5, kidney; 6, testis. (*c*) RT-PCR analysis of GOPCα and GOPCβ. One microgram of poly(A)$^+$ RNA were used for RT-PCR analysis. The fragments sized 201 bp and 177 bp represent GOPCα and GOPCβ, respectively. 1, brain; 2, liver; 3, kidney; 4, testis. (*d*) Immunoblot analysis of GOPC. Twenty-five-microgram aliquots of total lysates were analyzed with the anti-GOPC antibody. Lanes: 1, cerebrum; 2, cerebellum; 3, liver; 4, kidney; 5, testis.

Results

To investigate the physiological functions of GOPC in the mouse, we first analyzed the structure of cDNAs and their tissue expression. We have isolated several cDNAs that contained different 3′ untranslated fragments, resulting in 3.5- and 4.5-kb molecules. In the coding sequence, two splicing variants, GOPCα and GOPCβ, were identified, GOPCβ containing an additional 8-aa insertion encoded by exon 2b as compared with GOPCα (Figs. 1*a* and 2*a*). In Northern blot analysis, two bands, 3.5 kb and 4.5 kb, corresponding to two different 3′ untranslated fragments, were detected and GOPC was expressed in all tissues examined (Fig. 1*b*). To distinguish GOPCα and GOPCβ, we prepared a set of primers located in exons 2 and 3 and performed an RT-PCR analysis (Fig. 1*c*). GOPCβ was dominantly expressed in brain, whereas GOPCα was the major transcript in the other tissues. Similar results were obtained by RT-PCR analysis using different sets of primers (data not shown). Consistent with this result, in immunoblotting analysis using an anti-GOPC antibody that recognizes both GOPCα and GOPCβ, a slower-migrating band corresponding to GOPCβ was detected in the brain, whereas one for GOPCα was detected in other tissues examined (Fig. 1*d*).

To further address functional roles, we generated GOPC-deficient mice by gene targeting. A *GOPC*-targeting construct was designed to replace a 3.5-kb genomic region containing exons 2, 2b, and 3 by nLacZ and the floxed neomycin-resistance gene (*neo*^{r}) (Fig. 2). Homologous recombination should result in a protein consisting of the N-terminal 103 aa of the GOPC protein fused in frame with the nLacZ protein. We identified embryonic stem (ES) cell clones bearing the targeted allele by

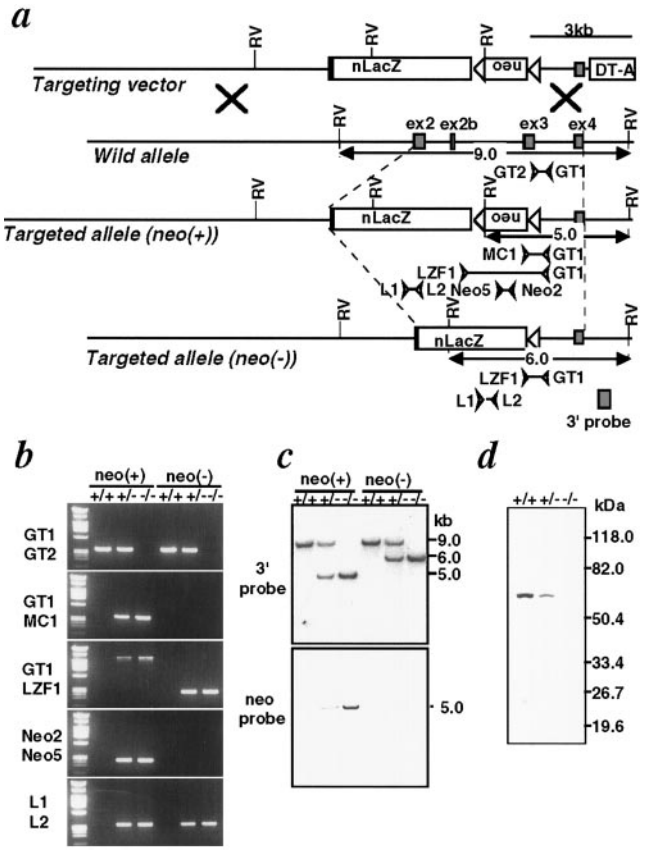

Fig. 2. Targeted disruption of the *GOPC* gene. (*a*) Schematic diagram of the targeting vector and the wild-type, targeted allele neo(+) and targeted allele neo(−). Exons 2, 2b, 3, and 4 of the *GOPC* gene are indicated by black boxes. The lox sequences are indicated by open triangles. Primers are shown as arrowheads. nLacZ, lacZ coding sequence with the nuclear localization signal; neo, neomycin-resistance gene driven by the thymidine kinase promoter; DT-A, diphtheria toxin A-chain gene; RV, *Eco*RV cleavage site. (*b*) PCR analysis of genomic DNA from *GOPC* mice. +/+, wild-type; +/−, heterozygote; −/−, homozygote; neo(+), targeted allele [neo(+)]; neo(−), targeted allele [neo(−)]. Primer sets used for the amplification are indicated. (*c*) Southern blot analysis of *Eco*RV-digested genomic DNA from *GOPC* mice. The location of the 3′ probe is shown in *a*. A 688-bp *Pst*I fragment of pMC1neo was used as a neo probe. (*d*) Immunoblot analysis of the *GOPC* mice. Total protein lysates (25 μg) from testes were analyzed with the anti-GOPC antibody.

Southern blot analysis and PCR analysis (data not shown). Two of them were used to generate chimeric mice featuring germline transmission of the targeted *GOPC* allele, and their offspring were used here. To generate homozygous mutant mice ($GOPC^{-/-}$), F_1 heterozygotes ($GOPC^{+/-}$) were interbred and the F_2 offspring were genotyped by PCR analysis and Southern blot analysis (Fig. 2 *b* and *c*). To exclude the possibility that the expression of neo^r may result in any particular phenotype, we crossed male chimeric mice with CAG-Cre females expressing Cre recombinase to generate a neo(−) targeted allele (10). The floxed neo^r was deleted by this cross, and offspring that did not contain the Cre gene were used for further studies. Mutant mice carrying both neo(+) targeted and neo(−) targeted alleles were analyzed, and similar results were obtained. Complete loss of GOPC protein in $GOPC^{-/-}$ mice was confirmed by immunoblot analysis (Fig. 2*d*).

Interbreeding of F1 $GOPC^{+/-}$ mice yielded F_2 offspring at the normal Mendelian ratio and $GOPC^{-/-}$ mice showed no overt abnormalities. In breeding experiments, although female fertility did not appear to be affected, male $GOPC^{-/-}$ mice were consistently infertile. Grossly, testes were normal in size (100 ± 9 mg for $GOPC^{-/-}$ mice vs. 117 ± 10 mg for $GOPC^{+/-}$ mice at 20 weeks) and the numbers of epididymal spermatozoa were similar to those of controls ($2.0 \pm 0.2 \times 10^7$ for $GOPC^{-/-}$ mice vs. $1.8 \pm 0.3 \times 10^7$ for $GOPC^{+/-}$ mice at 20 weeks). However, motility of sperm from $GOPC^{-/-}$ mice was significantly decreased (6.9 ± 4.4% for $GOPC^{-/-}$ mice vs. 59.3 ± 7.5% for $GOPC^{+/-}$ mice at 20 weeks). Most of the motile spermatozoa from $GOPC^{-/-}$ mice displayed only sluggish movement. In addition, an abnormal morphology of spermatozoa in the epididymides was evident by light microscopic examination using Nomarski optics (Fig. 3 *a–d*). In $GOPC^{+/+}$ and $GOPC^{+/-}$ mice, more than 95% of spermatozoa showed the characteristic hooked-head morphology (Fig. 3*a*), whereas all spermatozoa examined in $GOPC^{-/-}$ mice exhibited a round or ovoid shape (Fig. 3 *b–d*). A number of spermatozoa were seen to have their tails coiled around their nuclei (Fig. 3*b*). Similar morphological defects were also detected in mature spermatids in $GOPC^{-/-}$ testes (Fig. 3*f*). To elucidate the molecular basis for these phenotypes, we examined the expression and subcellular localization of GOPC protein in the testes. With immunohistochemistry, although GOPC was not detected in the outermost or basal layer of the seminiferous tubules, suggesting no expression in spermatogonia or Sertoli cells, spermatocytes and round spermatids were positively stained (Fig. 3*i*). In spermatocytes, GOPC was localized in the cytoplasm, whereas, in round spermatids, it was exclusively found in the perinuclear region (Fig. 3*i*). No signals were detected in $GOPC^{-/-}$ mice, indicating that this staining was specific for GOPC protein (Fig. 3*j*). In mice deficient for the DNA mismatch repair gene, *MLH-1*, which lack spermatids because of meiotic pachytene arrest (11), inner or adluminal cells were stained, confirming a cytoplasmic localization of GOPC in spermatocytes (Fig. 3*k*). Detailed analysis of spermatogenic cells that were isolated, fixed, and stained with anti-GOPC antibody demonstrated perinuclear and cytoplasmic staining in spermatocytes, and the protein was found exclusively in the perinuclear region in round spermatids. However, in elongated spermatids, GOPC was localized in the cytoplasmic compartment, rather than in the perinuclear region (Fig. 3 *l* and *m*). Thus it appears that GOPC is first expressed in spermatocytes, translocates to the perinuclear region in round spermatids, and then becomes localized in the cytoplasmic compartment in elongated spermatids, which is reminiscent of the location of the Golgi apparatus. Given that GOPC was detected in the Golgi apparatus in tissue culture cells (6, 7), we conclude that the protein is localized in the Golgi apparatus in spermatids. This result was confirmed by immunoelectron microscopic study (Fig. 4*g*). The expression and subcellular localization of the GOPC protein support the idea that the morphological defects of elongated spermatids as well as spermatozoa in epididymides occur because of altered maturation processes. Consistent with this idea, no morphological abnormalities were noted in spermatogonia and spermatocytes, as well as round spermatids, indicating that the initiation of spermatogenesis and subsequent progression through the meiotic prophase and divisions were normal (Fig. 3 *e–h*).

To characterize the morphologic defects in the developing sperm cells in detail, we performed an electron microscopic study. The first defects were detected in early round spermatids, in which acrosomal caps appeared discontinuous in cross sections, indicating they were abnormally fragmented (Fig. 4*b*, arrow). It is of note that relatively large vesicles were often observed adjacent to fragmented regions of the developing acrosomes—i.e., the acrosomal head caps (Fig. 4*b Inset*). In elongated spermatids, the morphological defects became more evident, with vacuolized acrosomes as well as examples with lost adhesion to the nucleus being observed (Fig. 4*d*, arrow). In some cases, complete loss of acrosomes was evident. In addition, all

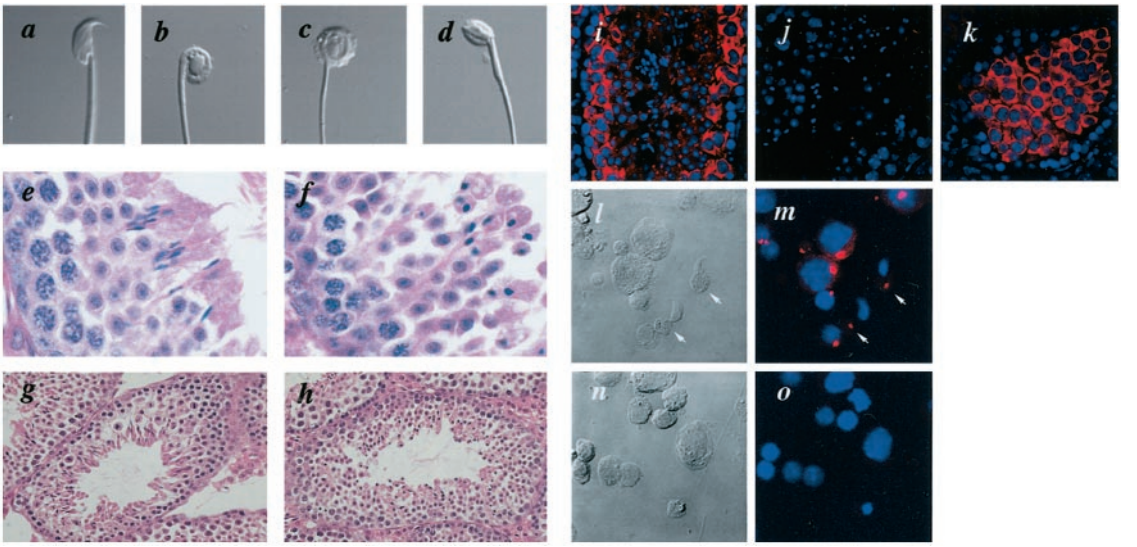

Fig. 3. Morphology of spermatogenic cells of wild-type and *GOPC* $^{-/-}$ mice and expression and subcellular localization of the GOPC protein. (*a–d*) Morphology of spermatozoa from wild-type (*a*) and *GOPC*$^{-/-}$ (*b–d*) mice. The spermatozoa were collected from the cauda epididymides, and photographed without fixation with Nomarski optics. (*e–h*) Histological sections of testis were stained with hematoxylin and eosin. The panels to the left (*e* and *g*) show histology of wild-type mice; those to the right (*f* and *h*), *GOPC*$^{-/-}$ mice. (*i–k)* Immunohistochemistry of GOPC in mouse testis. Sections from wild-type (*i*), *GOPC*$^{-/-}$ (*j*), and *Mlh-1*$^{-/-}$ (*k*) mice were stained with anti-GOPC antibody. Nuclei were stained with 4′,6-diamidino-2-phenylindole (DAPI). (*l–o*) Localization of GOPC in testis cells. Testis cells were prepared from wild-type (*l* and *n*) or *GOPC*$^{-/-}$ (*m* and *o*) mice, fixed on coverslips with methanol, and stained with anti-GOPC antibody followed by Cy3-conjugated anti-rabbit IgG. Nuclei were stained with DAPI. Nomarski optics images (*l* and *n*) and their corresponding fluorescence images (*m* and *o*) are shown. Arrows indicate GOPC staining in the cytoplasmic compartment (*a–d*, ×600; *e* and *f*, ×400; *g* and *h*, ×100; *i–k*, ×150; *l–o*, ×250.).

nuclei were malformed and showed a round or ovoid morphology. Occasional vacuole formation or invagination that gave the nucleus a crescent-shaped structure was apparent (Fig. 4*d*, arrowhead). These morphological defects, the loss of acrosomes and the malformation of nuclei, were also observed in epididymal sections (Fig. 4*f*). In addition, an abnormal arrangement of mitochondria in the mitochondrial sheath, which is located in the midpiece of the flagellum in normal spermatoza, was noted (Fig. 4*f Inset*). We next determined the subcellular localization of GOPC by immunoelectron microscopy in early round spermatids where the first defect in *GOPC*$^{-/-}$ mice was observed, and found the GOPC protein to be linked to the Golgi apparatus (Fig. 4*g*), the strongest signals being observed in trans-Golgi cisternae as well as the trans-Golgi network (Fig. 4*g Inset*). Importantly, we noticed signals in the medulla of round spermatids. Although the detailed localization of GOPC in the medulla needs to be determined, we often observed intense staining which was apparently associated with the Golgi-derived transport vesicles (Fig. 4*h*, arrows). No staining was observed in the Golgi apparatus or in medulla of *GOPC* $^{-/-}$ mice, indicating that these stainings were specific for GOPC protein. It is of note that no signals were detected in acrosomes (Fig. 4*g*).

Finally, we assessed defects of spermatozoa in *GOPC*$^{-/-}$ mice by *in vitro* fertilization (IVF). Because all spermatozoa in *GOPC*$^{-/-}$ mice lacked acrosomes, we assumed that they could not penetrate oocytes, and therefore used ICSI rather than conventional IVF (Table 1) (9). In the first ICSI cycle, only 4 of 21 surviving oocytes (19%) were fertilized, as assessed at 6 h after injection. Three oocytes had two pronuclei and two polar bodies, but none demonstrated normal cleavage. In the second ICSI cycle, when electroporation was performed on injected oocytes (9), 17 of 20 surviving oocytes (85%) showed signs of oocyte activation and 14 of these had two pronuclei and two polar bodies, 9 going on to cleave and develop into blastocysts. These results indicate that spermatozoa in *GOPC*$^{-/-}$ mice lack the ability to activate oocytes. The finding that activated oocytes are capable of participating in early developmental events is consistent with the observation of the normal initiation of spermatogenesis and subsequent progression through the meiotic prophase and divisions in *GOPC*$^{-/-}$ mice.

Discussion

GOPC is localized at the Golgi apparatus in tissue culture cells (6, 7), and it is present in the trans-Golgi cisternae as well as the trans-Golgi network in spermatids. In this study, we found that the acrosome was completely lost in the spermatozoa of *GOPC*$^{-/-}$ mice, and the primary defect of acrosome formation seemed to be the fragmentation of the acrosomal cap in early round spermatids (Fig. 4*b*, arrows). Interestingly, relatively large vesicles were often observed adjacent to fragmented regions of the acrosomal cap in *GOPC*$^{-/-}$ mice (Fig. 4*b Inset*). These abnormal vesicles were observed in as early as step 2–3 spermatids when the acrosome is not formed. Thus, these large vesicles are not the fragmented acrosome, and most likely are caused by defective fusion of the Golgi-derived transport vesicles to the acrosomal cap. Furthermore, we found that GOPC was localized in the medulla of round spermatids as well as at the trans-Golgi cisternae. Although the detailed localization of the GOPC in the medulla needs to be determined, these findings raise the possibility that GOPC may play a role in the fusion of transport vesicles to the acrosome. It is well documented that acrosomes are formed by the fusion of Golgi-derived vesicles, but the molecular mechanisms underlying the acrosome formation are largely unknown. We are not aware of any other Golgi-associated molecule besides GOPC that is required for acrosome formation.

GOPC was originally isolated as a Frizzled-interacting protein and was proposed to play a role in the vesicular transport from the Golgi apparatus to the plasma membrane (6). Recently, Cheng *et al.* (12) reported that a human homologue of GOPC bound to plasma membrane protein, CFTR(cystic fibrosis transmembrane conductance regulator), and modulated its plasma membrane expression, supporting the idea that GOPC plays a role in the vesicle transport from the Golgi apparatus to the

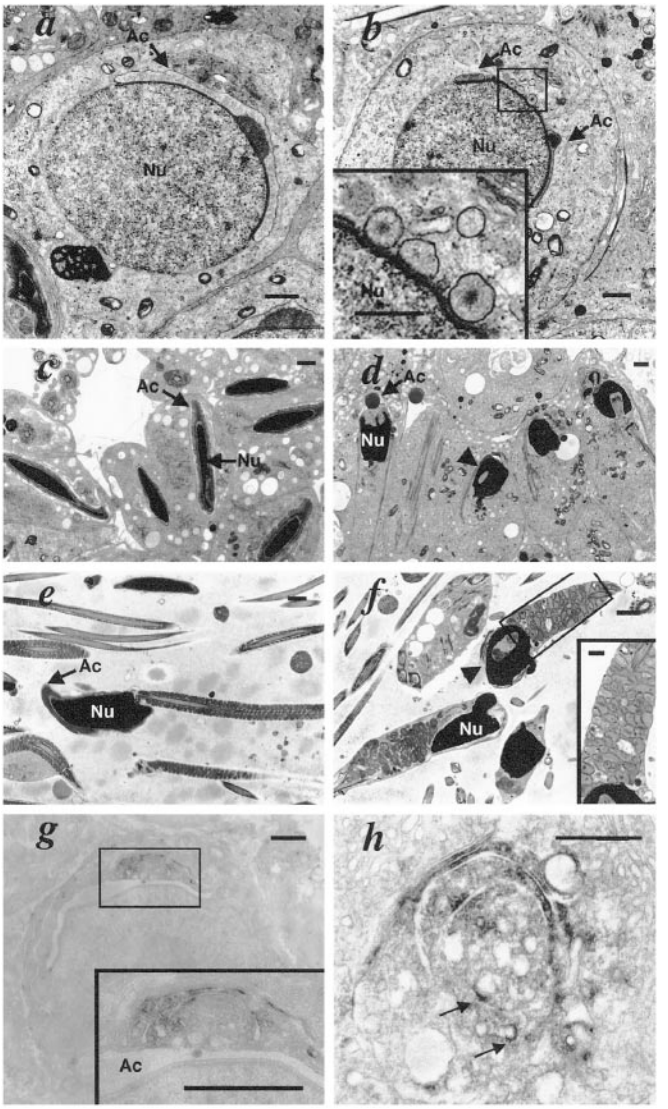

Fig. 4. Ultrastructural analysis of spermatogenic cells from wild-type and GOPC$^{-/-}$ mice. (*a–f*) Transmission electron microscopic features of the spermatogenic cells. The panels to the left (*a, c,* and *e*) show sections from wild-type mice; those to the right (*b, d,* and *f*) are from *GOPC*$^{-/-}$ mice. (*a*) In step 6 spermatids in wild-type mice, a cap-like acrosome was formed around the nucleus as indicated by an arrow. Ac, acrosome; Nu, nucleus. (Bar = 1 μm.) (*b*) In step 6 spermatids in *GOPC*$^{-/-}$ mice, the developing acrosome is fragmented, as indicated by arrows, and ill-developed or abnormally large vesicles which are not observed in wild-type spermatid were apparent (*Inset*). This abnormality was detected in as early as step 2–3 spermatids (not shown). (Bar = 1 μm; *Inset*: bar = 0.5 μm.) (*c*) In elongating spermatids in wild-type mice, chromosomes become condensed, nuclei become elongated, and acrosomes expand around the nucleus. (Bar = 1 μm.) (*d*) In GOPC$^{-/-}$ spermatids, although chromosome condensation is observed, nuclei are still ovoid. The arrowhead points to the vacuolized nucleus. Abnormalities of acrosomes including vacuolization, loss of adhesion to the nucleus, and total loss are apparent. (Bar = 1 μm.) (*e*) Wild-type spermatozoa exhibit the characteristic hooked shape. (Bar = 1 μm.) (*f*) In GOPC$^{-/-}$ epididymal spermatozoa, acrosomes are lost and nuclei are ovoid. The arrowhead points to the vacuolized nucleus. An abnormal arrangement of mitochondria in the mitochondrial sheath is also evident (*Inset*). (Bar = 1 μm; *Inset*: bar = 0.5 μm.) (*g* and *h*) Immunoelectron microscopic analysis of a round spermatid. GOPC is localized at the Golgi apparatus (*g*). Magnification of the rectangular region in *g* indicates the GOPC protein to be localized in trans-Golgi cisternae and the trans-Golgi network. Note that no signals were detected in the acrosome (Ac) (*g*), and GOPC proteins were often detected in the medulla of round spermatids, which were apparently associated with vesicle structures as indicated by arrows (*h*). (Bars = 1 μm for *g* and its *Inset*; bar = 0.5 μm for *h*.)

plasma membrane. Furthermore, the human homologue of GOPC was also shown to interact with syntaxin 6 (7). Because syntaxin 6 was suggested to function in tethering of post-Golgi vesicles to early endosome (13), GOPC may also implicated in Golgi–endosome transport (7). Thus it is likely that GOPC plays a multiple role besides the acrosome formation. Consistent with this possibility, GOPC is expressed all tissues examined in mice as well as in humans (6, 7, 12).

Unexpectedly, no overt abnormalities other than spermatogenesis in *GOPC*$^{-/-}$ mice were noted. Similarly, indirect immunofluorescence for the Golgi marker, the Golgi 58-kDa protein, and the recycling endosome marker, transferin receptor, was performed on wild-type and *GOPC*$^{-/-}$ mouse embryo fibroblasts, but the extent and pattern of these structures were comparable (data not shown). Furthermore, in electron microscopic study, we noticed that the structures of the Golgi apparatus as well as lysosomes were not significantly affected in *GOPC*$^{-/-}$ mice (data not shown). These results suggest the existence of a functionally redundant molecule or molecules that is not expressed in spermatids. Alternately, because the acrosome is a unique organelle, it is also possible that unidentified molecule or molecules that have an exclusive role in the acrosome formation in spermatids, but not in other cells, may require GOPC for acrosome formation. GOPC contains one PDZ domain and two coiled-coil motifs, both of which mediate interaction with other molecules. It would be interesting to determine the interacting molecule(s) of GOPC in spermatids.

Spermatogenesis has been found to be blocked in step 1 round spermatids of cAMP-responsive element modulator (CREM)-deficient mice, resulting in the complete lack of spermatozoa, with several genes that are required for the involved processes being targets of CREM (14, 15). However, CREM is first expressed in postmeiotic germ cells, whereas GOPC is already found in spermatocytes, so it is unlikely that GOPC is a downstream target of CREM. Disruption of the *CK2α′* gene results in nucleus malformation, but the primary defect is a specific abnormality of anterior head shaping in elongating spermatids and no abnormalities are detected until step 8 round spermatids (16). The spontaneous mutant mouse *azh* exhibits abnormalities in the formation of the manchette microtubules, but again no defects are seen until step 10 of spermatogenesis (17). In contrast, we observed defects of spermatogenesis in *GOPC*$^{-/-}$ mice at stages as early as step 2–3 spermatids, in which the fragmentation of acrosomal caps was already evident. Thus, the defects observed in *GOPC*$^{-/-}$ mice are distinct from those described in other mutants and therefore may provide important clues to understanding the mechanisms underlying spermatogenesis.

Hrb is an Asn-Pro-Phe (NPF) motif-containing protein that has been shown to interact with Eps15, a transport vesicle adaptor protein (18). Recently, Kang-Decker *et al.* (19) reported that Hrb-deficient mice lack acrosome formation. The primary defect in the spermatogenesis of Hrb-deficient mice was an arrest in the acrosomic vesicle biogenesis at step 2 of spermatogenesis, and numerous small proacrosomic vesicles that failed to fuse with each other were observed. This phenotype is reminiscent of that observed in GOPC-deficient mice. It is important to note that Hrb was localized at the outer membrane of the acrosome, where GOPC was not detected. GOPC was localized at the Golgi apparatus as well as at the medulla of the early round spermatids. Because both Hrb and GOPC are suggested to function in vesicle-to-vesicle docking and/or fusion during acrosome biogenesis, it may be interesting to investigate the possible interaction of Hrb and GOPC.

In *GOPC*$^{-/-}$ mice, in addition to the lack of acrosomes, malformation of the nucleus was observed. Although such morphological defects might not be caused directly by GOPC deficiency, they are reminiscent of those described in human

Table 1. Fertilization and developmental ability of mouse oocytes injected with spermatozoa from *GOPC* wild-type, heterozygous, and homozygous mice

Sperm injected	No. of oocytes injected	No. (%) of oocytes surviving	No. (%) of activated eggs	No. (%) of eggs with			No. of oocytes cultured	No. (%) of eggs developed to			
				2PN + 2pb	3PN	Other		2-cell	4-cell	Morula	Blastocyst
Wild-type [EP(−)]	28	19 (68)	19 (100)	19 (100)	0 (0)	0 (0)	11	11 (100)	11 (100)	11 (100)	11 (100)
Heterozygous [EP(−)]	24	12 (50)	10 (83)	10 (100)	0 (0)	0 (0)			ND		
Homozygous [EP(−)]	36	21 (58)	4 (19)	3 (75)	1 (25)	0 (0)	3	0 (0)	0 (0)	0 (0)	0 (0)
Homozygous [EP(+)]	40	20 (50)	17 (85)	14 (82)	2 (12)	1 (7)	14	12 (86)	9 (64)	9 (64)	9 (64)

ND, not determined; EP, electroporation; PN, pronuclei; pb, polar bodies.

globozoospermia (2–4). This is an inherited disorder with the signature characteristics of round-headed spermatozoa and a lack of acrosomes. The abnormal arrangement of mitochondria in the mitochondrial sheath of spermatozoa observed in *GOPC*$^{-/-}$ mice has also been reported in human globozoospermia (4). Interestingly, round-headed spermatozoa are deficient in the oocyte-activation capacity independent of variation in morphology (20). These findings raise the possibility that GOPC may be responsible for at least some cases of human globozoospermia. Several etiologies have been proposed, including a failure of acrosomes to develop and a disrupted normal development of the nuclear matrix or manchettes (4). The results obtained in this study suggest that the primary defect in *GOP* $^{-/-}$ mice is the failure of acrosomes to develop and hence to taper the nucleus to a conical extremity. Thus, the *GOPC*$^{-/-}$ mouse may be a unique and valuable model for human globozoospermia.

This work was supported by a grant-in-aid for Scientific Research on Priority Areas (to R.Y. and T.N.) from the Ministry of Education, Culture, Sports, Science, and Technology.

1. Abou, H. A. & Tulsiani, D. R. (2000) *Arch. Biochem. Biophys.* **379,** 173–182.
2. Kullander, S. & Rausing, A. (1975) *Int. J. Fertil.* **20,** 33–40.
3. Lalonde, L., Langlais, J., Antaki, P., Chapdelaine, A., Roberts, K. D. & Bleau, G. (1988) *Fertil. Steril.* **49,** 316–321.
4. Singh, G. (1992) *Int. J. Fertil.* **37,** 99–102.
5. Battaglia, D. E., Koehler, J. K., Klein, N. A. & Tucker, M. J. (1997) *Fertil. Steril.* **68,** 118–122.
6. Yao, R., Maeda, T., Takada, S. & Noda, T. (2001) *Biochem. Biophys. Res. Commun.* **286,** 771–778.
7. Charest, A., Lane, K., McMahon, K. & Housman, D. E. (2001) *J. Biol. Chem.* **276,** 29456–29465.
8. Bellve, A. R. (1993) in *Guide to Techniques in Mouse Development,* eds. Wassarman, P. W. & Depamphilis, M. L. (Academic, San Diego), pp. 84–113.
9. Kimura, Y. & Yanagimachi, R. (1995) *Biol. Reprod.* **52,** 709–720.
10. Sakai, K. & Miyazaki, J. I. (1997) *Biochem. Biophys. Res. Commun.* **237,** 318–324.
11. Edelmann, W., Cohen, P. E., Kane, M., Lau, K., Morrow, B., Bennett, S., Umar, A., Kunkel, T., Cattoretti, G., Chaganti, R., *et al.* (1996) *Cell* **85,** 1125–1134.
12. Cheng, J., Moyer, B. D., Milewski, M., Loffing, J., Ikeda, M., Mickle, J. E., Cutting, G. R., Li, M., Stanton, B. A. & Guggino, W. B. (2002) *J. Biol. Chem.* **277,** 3520–3529.
13. Simonsen, A., Gaullier, J. M., D'Arrigo, A. & Stenmark, H. (1999) *J. Biol. Chem.* **274,** 28857–28860.
14. Blendy, J. A., Kaestner, K. H., Weinbauer, G. F., Nieschlag, E. & Schutz, G. (1996) *Nature (London)* **380,** 162–165.
15. Nantel, F., Monaco, L., Foulkes, N. S., Masquilier, D., LeMeur, M., Henriksen, K., Dierich, A., Parvinen, M. & Sassone, C. P. (1996) *Nature (London)* **380,** 159–162.
16. Xu, X., Toselli, P. A., Russell, L. D. & Seldin, D. C. (1999) *Nat. Genet.* **23,** 118–121.
17. Cole, A., Meistrich, M. L., Cherry, L. M. & Trostle, W. P. (1988) *Biol. Reprod.* **38,** 385–401.
18. Salcini, A. E., Confalonieri, S., Doria, M., Santolini, E., Tassi, E., Minenkova, O., Cesareni, G., Pelicci, P. G. & Di, F. P. (1997) *Genes Dev.* **11,** 2239–2249.
19. Kang-Decker, N., Mantchev, G. T., Juneja, S. C., McNiven, M. A. & van Deursen, J. M. A. (2001) *Science* **294,** 1531–1533.
20. Rybouchkin, A., Dozortsev, D., Pelinck, M. J., De Sutter, P. & Dhont, M. (1996) *Hum. Reprod.* **11,** 2170–2175.